PCCP

Accepted Manuscript

ROYAL SOCIETY OF CHEMISTRY

www.rsc.org/pccp

Gradual Plasmon Evolution and Huge Infrared Near-field Enhancement of Metallic Bridged Nanoparticle Dimers†

Yu Huang,[a] Lingwei Ma,[a] Mengjing Hou,[a] Zheng Xie[b] and Zhengjun Zhang*[,c]

[a] *State Key Laboratory of New Ceramics and Fine Processing, School of Materials Science and Engineering, Tsinghua University, Beijing 100084, P. R. China*

[b] *High-Tech Institute of Xi'an, Shaanxi 710025, P.R. China*

[c] *Key Laboratory of Advanced Materials (MOE), School of Materials Science and Engineering, Tsinghua University, Beijing 100084, P. R. China. E-mail: zjzhang@mail.tsinghua.edu.cn*

† Electronic Supplementary Information (ESI) available. See DOI: 10.1039/

Graphical abstract

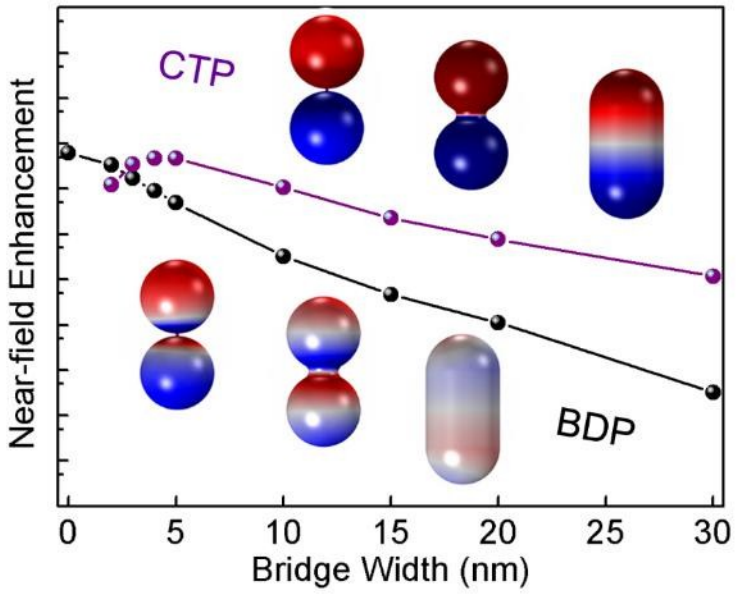

Gradual plasmon evolutions of BDP and CTP modes are visualized. Particularly, the CTP mode enables huge infrared near-field enhancement.

Abstract

By three dimensional (3D) finite element method (FEM) plasmon mapping, gradual plasmon evolutions of both bonding dipole plasmon (BDP) and charge transfer plasmon (CTP) modes are visualized. In particular, the evolved BDP mode provides a physical insight into the rapid degeneration of electromagnetic hot spots in practical applications, while the rising CTP mode enables huge near-field enhancement for potential plasmonic devices at infrared wavelengths.

Manuscript text

In plasmonics, it is well-known that metallic nanoparticles, usually of Ag or Au, can undergo light-driven collective oscillations of the conduction electrons, i.e., localized surface plasmon resonances (LSPRs). By virtue of being small, such particles are able to concentrate and guide light at the sub-wavelength scale[1] and provide extremely large localized near-field enhancements.[2] These unique properties benefit applications in a wide variety of fields such as plasmonic waveguiding,[3] surface enhanced Raman and infrared spectroscopies,[4-8] chemical and biological sensing,[9-11] and so on. Understanding and predicting the fundamental physics governing LSPRs are both necessary to realize and fully optimize potential plasmonic devices. Among the most geometrically simple but plasmonically important structures is the dimer, consisting of two metallic nanoparticles separated by a small gap.[12,13] Usually, the dipole plasmons of individual nanoparticles hybridize to form the bonding dipole plasmon (BDP) mode,[14,15] enabling special applications ranging from single molecule detection[16,17] to

nonlinear optics,[18,19] due to the enormous electromagnetic (EM) field confinement and enhancement at the nanogap known as hot spots.

Another profound aspect of metallic nanoparticle dimers concerns the regime where the two particles are conductively bridged, giving rise to the so-called charge transfer plasmon (CTP) mode at lower energies (longer wavelengths).[20-22] This mode involves the flow of conduction electrons through the junction and thus the transfer of net charge between the two particles. The onset of CTP can result in a drastic modification in both the near- and far-field plasmonic properties of the structure,[23-26] which could have broad applications in nanoelectronics, optoelectronics and active plasmonic devices.[27-29] The CTP can also be supported by plasmonic dimers with very small gaps less than 0.4 nm.[30] In that case, the free electrons can directly tunnel through the flat energy barrier between the particles, which has recently opened up new prospects in the field of quantum plasmonics.[31-35]

Here, we numerically study the near- and far-field plasmonic properties of metallic bridged nanoparticle dimers. By mapping three dimensional (3D) surface charge distributions directly, we visualize a gradual evolution of both BDP and CTP modes toward common plasmon modes found in single nanorod structures. It is then revealed that the near-field enhancement sustained by the BDP mode decreases almost exponentially as the bridge width increases, which provides a physical insight into the rapid degeneration of EM hot spots in practical applications owing to thermal coarsening of metallic nanostructures. Meanwhile the BDP mode enables an enormous near-field enhancement with good tunability in near-infrared and mid-infrared regions, offering a new approach to engineering plasmonic devices at infrared wavelengths.

For spectroscopy applications, we further demonstrate that the near- and far-field optical responses of the considered models correlate with each other.

Frequency-domain finite element method (FEM) in COMSOL Multiphysics software package[36] (installed on a Quad Intel Xeon CPU, 64 GB RAM workstation) was performed for our 3D electrodynamic calculations. Typically, the model of the dimer structure consists of two Ag nanoparticles (radius R = 30 nm) separated by 2 nm gap and bridged by a thin Ag junction. As is shown in the inset of Fig. 1a, the bridge junction is the shape of a truncated cylinder with radius r ranging from 0 to 30 nm. For the consideration of physical stability, the junction is smoothed by an arc tangent to the two paricles. Actually a bridged dimer can be treated as the intermediate case between a nonbridged dimer (r = 0 nm in our modeling) and a smooth nanorod ($r = R$ = 30 nm).

In the process of computation the dielectric function $\varepsilon(w)$ of Ag is modeled by a Lorentz-Drude dispersion model[37] fitting the experimental data in Palik's book:[38]

$$\varepsilon(w) = 1 - \frac{f_0 {w_p}^2}{w(w - i\Gamma_0)} + \sum_{j=1}^{m} \frac{f_j {w_p}^2}{({w_j}^2 - w^2) + iw\Gamma_j}, \quad (1)$$

where w_p is the plasma frequency with oscillator strength f_0 and damping constant Γ_0. The last term of Eq. 1 is the result of the Lorentz modification, where m is the number of oscillators with frequency w_j, strength f_j and damping constant Γ_j. The fitting parameter values are f_0 = 0.845, w_p = 9.01 eV, Γ_0 = 0.048 eV, f_1 = 0.065, Γ_1 = 3.886 eV, w_1 = 0.816 eV, f_2 = 0.124, Γ_2 = 0.452 eV, w_2 = 4.481 eV, f_3 = 0.011, Γ_3 = 0.065 eV, w_3 = 8.185 eV, f_4 = 0.840, Γ_4 = 0.926 eV, w_4 = 9.083 eV, f_5 = 5.646, Γ_5 = 2.419 eV, w_5 = 20.29 eV.

A self-defined near-field enhancement spectroscopy is applied to extract the resonance energy where a maximum near field enhancement is achieved.[12,39] The spectroscopy is represented by the averaged local electric field enhancement factor (EF = $|E/E_0|^4$):

$$\overline{EF} = \frac{\iiint (|\boldsymbol{E}|^4/|\boldsymbol{E}_o|^4)\, dV}{V}, \quad (2)$$

where V is the volume within a certain distance above the metal surface (here we take 2 nm),[39] the modulus of incident field $|E_0|$ = 1 V/m and $\boldsymbol{E}$ = (E_x, E_y, E_z) is the local electric field. It is known that the EF of SERS is nearly proportional to the forth power of the local electric field intensity.[40,41] Thus the physical significance of $\overline{EF}$ can be understood as the averaged EM EF of surface enhanced Raman scattering (SERS),[40,42] on the assumption that Raman probe molecules are arranged randomly and uniformly at the surface of metallic nanoparticles. Instead of a surface integral, the volume integral is performed with consideration of numerical instabilities at the metal surface and dimensions of adsorbed molecules.[43] For far-field properties, extinction spectra were calculated by integrating the time-averaged extinction Poynting vectors (i.e. EM power flow) over an auxiliary surface enclosing the dimers.[12,39] Using adaptive meshing, the highest spatial resolution of the grid is 0.5 nm in the simulation. The computational time for an entire spectrum (i.e. ~300 spectral points) is ~24 h.

Fig. 1 shows the calculated far-field extinction cross section C_{ext} spectra and near-field $\overline{EF}$ spectra for varied birdge widths r. The incident polarization is along the interparticle axis. It is noticed that there are two pronounced resonance peaks at lower energies for each structure, with a one-to-one correspondence between the extinction and $\overline{EF}$ spectra. These peaks indicated by the dashed black and red lines are indentified to be the BDP and CTP modes respectively, which will be demonstrated in Fig. 2 and 3. The BDP mode is in the visible regime

(2.56-3.40 eV, 485-370 nm) while the CTP mode is tuned from the visible regime to the mid-infrared regime (0.39-2.32 eV, 3160-535 nm).

For the BDP modes, typical local electric field distributions at the resonance energies are shown in the upper panels of Fig. 2, in the form of logarithmic $|E/E_0|^4$. Fig. 2a-d correspond to r = 2, 5, 15, 30 nm from left to right. The local fields near the metallic junction are extremely enhanced for r = 2 nm, reaching up to an order of 10^9 in terms of $|E/E_0|^4$; however, the maximum $|E/E_0|^4$ for the smooth nanorod (r = 30 nm) decreases rapidly, to an order of 10^2.

To confirm the plasmon modes, 3D surface charge distributions are calculated by applying Gauss' law during the simulation. The Gauss' law in the integral form is:

$$\Phi_E = \frac{Q}{\varepsilon_0} = \oiint_S (\boldsymbol{n} \cdot \boldsymbol{E})\, dS, \quad (3)$$

where Φ_E is the electric flux through the metal surface S, Q is the total charge, ε_0 is the permittivity of vacuum, $\boldsymbol{n} = (n_x, n_y, n_z)$ is the outward normal vector of the metal surface and $\boldsymbol{E} = (E_x, E_y, E_z)$ is the local electric field. Since metals like Ag and Au are good electrical conductors and hence almost all the induced charge distributes on the particle surface, thus $Q = \oiint_S \rho\, dS$, where ρ is the surface charge density. It can then be deduced:

$$\rho = \varepsilon_0 \cdot (\boldsymbol{n} \cdot \boldsymbol{E}) = \varepsilon_0 \cdot (n_x \cdot E_x + n_y \cdot E_y + n_z \cdot E_z). \quad (4)$$

In the bottom panels of Fig. 2, the corresponding 3D surface charge distributions are plotted. It is worth mentioning that the plotted surface charge distributions are with the maximum transient charge polarizations within one full oscillation.[44] The strong correlation between the surface plasmon geometry and the local electric field distributions are observed. This mapping shows clearly the fundamental dipole mode for individual particles and the hybridized BDP

mode in terms of the whole structure. Seen from Fig. 2h, the BDP mode has evolved into a common mode which is exactly the third-order multipole plasmon modes for a nanorod, since there are four induced charge poles distributed alternately positive and negative.[45,46]

Fig. 3 shows the local electric field distributions and related 3D surface charge distributions for the CTP modes corresponding to each of above structures. Still, extremely enhanced local electric fields distribute around the narrow bridges, and decrease rapidly as *r* increases. Seen from the surface charge maps, it is no wonder that the CTP modes are sometimes understood as a hybridization of monopole modes.[25] Considering the entire structure, the CTP mode is actually the fundamental dipole mode, or the first-order plasmon mode. Interestingly there is no resonance peak between the BDP amd CTP mode in the spectra (Fig.1). It is because the second-order plasmon mode of a nanorod is forbidden at the perpendicular incidence.[46]

For further understanding on the near-field enhancement of bridged dimers, the peak $\overline{EF}$ values in Fig. 1b and the maximum EF (EF_{max}) values are extracted and plotted in Fig. 4a as a function of the bridge width *r*. For the BDP mode, the presence of metallic bridges decreases the electric field enhancement compared to that of a nonbridged dimer (*r* = 0 nm). Moreover, the $\overline{EF}$ decrease exponentially as *r* continues to increase. The corresponding EF_{max} values is found to be 1-3 orders of magnitude higher than the defined $\overline{EF}$ values while exhibiting a similar exponential decay, which means a rapid degeneration of hot spots. Usually in practical applications, due to the intrinsic surface diffusion of atoms, metallic nanostructures used as SERS substrates suffer from morphological instability and serious losses of hot spots, even near room temperature.[13,47] Here our models present a physical insight into this phenomenon, which may serve as an important guide for optimized design of practical plasmonic devices.

Indeed our results highlight the significance of enhanced thermal stability of metallic nanostructures.[47,48]

On the other hand, this exponential downward trend of near-field enhancement applies to the CTP mode as well when the bridge is wide enough. Unlike the case for the BDP mode, as r becomes further less (r < 4 nm), $\overline{EF}$ undergoes a modest decrease instead of an increase. The maximum $\overline{EF}$ = 4.7 × 10^6 (EF = 4.2 × 10^8) occurs when r = 4 nm. According to Gauss' law, the intensity of local electric field is positively related to the surface charge density. Comparing Fig. 3e with Fig. 3f and 3g, we can see the surface charge density is lower for the bridged dimer r = 2 nm. This can be qualitatively understood since the flow of conduction electrons is limited by the narrow bridge. It is worth mentioning that for the bridged dimers r = 2-10 nm, the peak $\overline{EF}$ stays in a very high level (> 10^6), EF_{max} > 2 × 10^6 while the resonance energy is tuned from 0.39 eV (3160 nm) to 1.35 eV (920 nm) as r increases to 10 nm (r/R = 1/3). This enormous and tunable infrared near-field enhancement offers a new approach to engineering plasmonic devices at near-infrared and mid-infrared wavelengths for applications like surface enhanced infrared absorption (SEIRA).[7,13,49] As is known, the infrared absorption scales with the second power of local electric field intensity. For the model r = 4 nm, the maximum $|E/E_0|^2$ is 2 × 10^4, which approaches surprisingly the SEIRA enhancement factor with an attomolar detection sensitivity (10^{-18} M).[50]

Meanwhile in practical applications, it has recently been fully appreciated that there exists a distinct deviation of spectral positions between the near- and far-field plasmonic responses as the near-field resonance is usually red-shifted compared to the far-field resonance, and in many cases only single frequencies are considered for near-field enhancement.[12,51,52] To consider the

deviation of our models here, the near- and far-field resonance energies are plotted in Fig. 4b as a function of *r*. It turns out that the near- and far-field resonances take place at nearly the same energies. Noticing the points in the plot: r = 20 nm for the BDP mode and r = 30 nm for the CTP mode, the maximum deviation in our models is only 10 nm. Thus the presence of a far-field extinction peak can be taken as direct evidence of an excitation energy (or wavelength) with a favorable maximum near-field enhancement. Besides, both the BDP and CTP modes exhibit a gradual blueshift as *r* continues to increase, which can be attributed to the increasing conductance of the bridged junction.[25-27] To be specific, the bridge conductance can be calculated as $G = \sigma(w)r^2/l$, where $\sigma(w)$ is the frequency dependent AC conductivity of the bridge material and l is the bridge length.[29] Concurrently, the resonance broader width of the CTP (Fig. 1) is a result of the increased radiation damping.[29]

In conclusion, we have performed a theoretical study of both the near- and far-field plasmonic properties of Ag nanoparticle dimers bridged by a smooth thin Ag junction. As the bridge width increase, the BDP mode evolves into the third-order multipole plasmon mode while the CTP mode can be viewed as the fundamental dipole mode. The presence of metallic bridges shifts the BDP and CTP modes to the blue. The near-field enhancement sustained by the BDP mode decreases almost exponentially as the bridge width increases, which provides a physical insight into the rapid degeneration of EM hot spots in practical applications owing to thermal coarsening of metallic nanostructures. Meanwhile the rising BDP mode enables an enormous infrared near-field enhancement which can be tuned by the bridge conductance, offering a new approach to engineering potential plasmonic devices at near-infrared and mid-infrared wavelengths. For spectroscopy applications, we further demonstrate that the near- and

far-field optical responses of our models correlate well with each other. Our results provide a comprehensive physical image of the metallic bridged nanoparticle dimer system necessary for fundamental studies and practical applications.

Acknowledgements

The authors thank Professor W.S. Lai for the access to COMSOL Multiphysics software. This work was supported by the National Basic Research Program of China (973 program, Grant No. 2013CB934301), the National Natural Science Foundation of China (Grant No. 51531006, 51572148), the Research Project of Chinese Ministry of Education (Grant No. 113007A), and the Tsinghua University Initiative Scientific Research Program.

Notes and references

1 D. K. Gramotnev and S. I. Bozhevolnyi, *Nat. Photonics*, 2014, 8, 13-22.

2 E. Hao and G. C. Schatz, *J. Chem. Phys.*, 2004, 120, 357-366.

3 S. I. Bozhevolnyi, V. S. Volkov, E. Devaux, J. Y. Laluet and T. W. Ebbesen, *Nature*, 2006, 440, 508-511.

4 J. F. Li, Y. F. Huang, Y. Ding, Z. L. Yang, S. B. Li, X. S. Zhou, F. R. Fan, W. Zhang, Z. Y. Zhou, D. Y. Wu, B. Ren, Z. L. Wang and Z. Q. Tian, *Nature*, 2010, 464, 392-395.

5 B. Sharma, R. R. Frontiera, A.-I. Henry, E. Ringe and R. P. Van Duyne, *Mater. Today*, 2012, 15, 16-25.

6 D. Brouard, M. L. Viger, A. G. Bracamonte and D. Boudreau, *ACS Nano*, 2011, 5, 1888-1896.

7 S. Lal, N. K. Grady, J. Kundu, C. S. Levin, J. B. Lassiter and N. J. Halas, *Chem. Soc. Rev.*, 2008, 37, 898-911.

8 Q. Zhou, X. Zhang, Y. Huang, Z. C. Li, Y. P. Zhao and Z. J. Zhang, *Appl. Phys. Lett.*, 2012, 100, 113101.

9 S. Lal, S. E. Clare and N. J. Halas, *Acc. Chem. Res.*, 2008, 41, 1842-1851.

10 Y.-L. Ho, L.-C. Huang, E. Lebrasseur, Y. Mita and J.-J. Delaunay, *Appl. Phys. Lett.*, 2014, 105, 061112.

11 A. Yang, M. D. Huntington, M. F. Cardinal, S. S. Masango, R. P. Van Duyne and T. W. Odom, *ACS Nano*, 2014, 8, 7639-7647.

12 Y. Huang, Q. Zhou, M. Hou, L. Ma and Z. Zhang, *Phys. Chem. Chem. Phys.*, 2015, 17, 29293-29298.

13 G. González-Rubio, J. González-Izquierdo, L. Bañares, G. Tardajos, A. Rivera, T. Altantzis, S. Bals, O. Peña-Rodríguez, A. Guerrero-Martínez and L. M. Liz-Marzán, *Nano Lett.*, 2015, 15, 8282-8288.

14 P. Nordlander, C. Oubre, E. Prodan, K. Li and M. I. Stockman, *Nano Lett.*, 2004, 4, 899-903.

15 E. Prodan, C. Radloff, N. J. Halas and P. Nordlander, *Science*, 2003, 302, 419-422.

16 S. Nie and S. R. Emory, *Science*, 1997, 275, 1102-1106.

17 K. Kneipp, Y. Wang, H. Kneipp, L. T. Perelman, I. Itzkan, R. Dasari and M. S. Feld, *Phys. Rev. Lett.*, 1997, 78, 1667-1670.

18 S. Kim, J. H. Jin, Y. J. Kim, I. Y. Park, Y. Kim and S. W. Kim, *Nature*, 2008, 453, 757-760.

19 H. Aouani, M. Rahmani, M. Navarro-Cia and S. A. Maier, *Nat. Nanotechnol.*, 2014, 9, 290-294.

20 T. Atay, J. H. Song and A. V. Nurmikko, *Nano Lett.*, 2004, 4, 1627-1631.

21 I. Romero, J. Aizpurua, G. W. Bryant and F. J. G. de Abajo, *Opt. Express*, 2006, 14, 9988-9999.

22 J. B. Lassiter, J. Aizpurua, L. I. Hernandez, D. W. Brandl, I. Romero, S. Lal, J. H. Hafner, P. Nordlander and N. J. Halas, *Nano Lett.*, 2008, 8, 1212-1218.

23 M. Schnell, A. Garcia-Etxarri, A. J. Huber, K. Crozier, J. Aizpurua and R. Hillenbrand, *Nat. Photonics*, 2009, 3, 287-291.

24 O. Perez-Gonzalez, N. Zabala and J. Aizpurua, *New J. Phys.*, 2011, 13, 083013.

25 L. F. Liu, Y. M. Wang, Z. Y. Fang and K. Zhao, *J. Chem. Phys.*, 2013, 139.

26 J. Fontana and B. R. Ratna, *Appl. Phys. Lett.*, 2014, 105, 011107.

27 O. Perez-Gonzalez, N. Zabala, A. G. Borisov, N. J. Halas, P. Nordlander and J. Aizpurua, *Nano Lett.*, 2010, 10, 3090-3095.

28 O. Perez-Gonzalez, J. Aizpurua and N. Zabala, *Opt. Express*, 2013, 21, 15847-15858.

29 F. F. Wen, Y. Zhang, S. Gottheim, N. S. King, Y. Zhang, P. Nordlander and N. J. Halas, *ACS Nano*, 2015, 9, 6428-6435.

30 J. Zuloaga, E. Prodan and P. Nordlander, *Nano Lett.*, 2009, 9, 887-891.

31 K. J. Savage, M. M. Hawkeye, R. Esteban, A. G. Borisov, J. Aizpurua and J. J. Baumberg, *Nature*, 2012, 491, 574-577.

32 L. Wu, H. G. Duan, P. Bai, M. Bosman, J. K. W. Yang and E. P. Li, *ACS Nano*, 2013, 7, 707-716.

33 S. F. Tan, L. Wu, J. K. W. Yang, P. Bai, M. Bosman and C. A. Nijhuis, *Science*, 2014, 343, 1496-1499.

34 V. Kulkarni and A. Manjavacas, *ACS Photonics*, 2015, 2, 987-992.

35 M. S. Tame, K. R. McEnery, S. K. Oezdemir, J. Lee, S. A. Maier and M. S. Kim, *Nat. Phys.*, 2013, 9, 329-340.

36 COMSOL Multiphysics, version 4.4, RF module, http://www.comsol.com.

37 A. D. Rakic, A. B. Djurisic, J. M. Elazar and M. L. Majewski, *Appl. Opt.*, 1998, 37, 5271-5283.

38 E. D. Palik, *Handbook of Optical Constants of Solid*, Academic Press, New York, 1985.

39 Y. Huang, E. Ringe, M. Hou, L. Ma and Z. Zhang, *AIP Advances*, 2015, 5.

40 F. J. GarciaVidal and J. B. Pendry, *Phys. Rev. Lett.*, 1996, 77, 1163-1166.

41 K. L. Wustholz, A. I. Henry, J. M. McMahon, R. G. Freeman, N. Valley, M. E. Piotti, M. J. Natan, G. C. Schatz and R. P. Van Duyne, *J. Am. Chem. Soc.*, 2010, 132, 10903-10910.

42 D. L. Jeanmaire and R. P. Van Duyne, *J. Electroanal. Chem.*, 1977, 84, 1-20.

43 K. D. Alexander, K. Skinner, S. Zhang, H. Wei and R. Lopez, *Nano Lett.*, 2010, 10, 4488-4493.

44 See the supplemental material for movies of surface charge distributions within one oscillation for the BDP and CTP mode of the bridged dimer r = 2 nm.

45 E. Ringe, B. Sharma, A. I. Henry, L. D. Marks and R. P. Van Duyne, *Phys. Chem. Chem. Phys.*, 2013, 15, 4110-4129.

46 E. Kazuma and T. Tatsuma, *J. Phys. Chem. C*, 2013, 117, 2435-2441.

47 L. Bachenheimer, P. Elliott, S. Stagon and H. Huang, *Appl. Phys. Lett.*, 2014, 105, 213104.

48 L. Ma, Y. Huang, M. Hou, Z. Xie and Z. Zhang, *Sci. Rep.*, 2015, 5, 12890.

49 C. Huck, F. Neubrech, J. Vogt, A. Toma, D. Gerbert, J. Katzmann, T. Haertling and A. Pucci, *ACS Nano*, 2014, 8, 4908-4914.

50 F. Neubrech, A. Pucci, T. W. Cornelius, S. Karim, A. Garcia-Etxarri and J. Aizpurua, *Phys. Rev. Lett.*, 2008, 101, 157403.

51 B. M. Ross and L. P. Lee, *Opt. Lett.*, 2009, 34, 896-898.

52 J. M. Sanz, D. Ortiz, R. Alcaraz de la Osa, J. M. Saiz, F. Gonzalez, A. S. Brown, M. Losurdo, H. O. Everitt and F. Moreno, *J. Phys. Chem. C*, 2013, 117, 19606-19615.

Fig Captions

Fig. 1 FEM calculated far-field extinction cross section C_{ext} (a) and corresponding near-field $\overline{EF}$ (b) spectra for Ag nanoparticle (R = 30 nm) dimers separated by 2 nm gap, and bridged by a thin Ag junction (the inset). The bridge width r varies from 0 to 30 nm. The incident polarization is along the interparticle axis.

Fig. 2 (Upper panels) (a)-(d) Typical local electric field distributions in the form of logarithmic $|E/E_0|^4$ for the BDP modes. From left to right, (a) r = 2 nm, (b) r = 5 nm, (c) r = 15 nm, and (d) r = 30 nm. (Bottom panels) (e)-(f) Corresponding 3D surface charge distributions. Red color represents positive charge while blue is negative.

Fig. 3 Local electric field and corresponding surface charge distributions for the CTP modes. The structures and mapping method are the same as in Fig. 2.

Fig. 4 (a) Extracted peak $\overline{EF}$ and EF_{max} values as a function of r for the BDP and CTP modes. The green lines represent least-squares fits to the exponential decay function. For the BDP mode, $\lg(\overline{EF}) = -0.178r + 6.626$ (r = 2-30 nm, R^2 = 0.983); For the CTP mode, $\lg(\overline{EF}) = -0.104r + 7.061$ (r = 5-30 nm, R^2 = 0.978). (b) Calculated near- and far-field resonance energies for both modes.

Figures

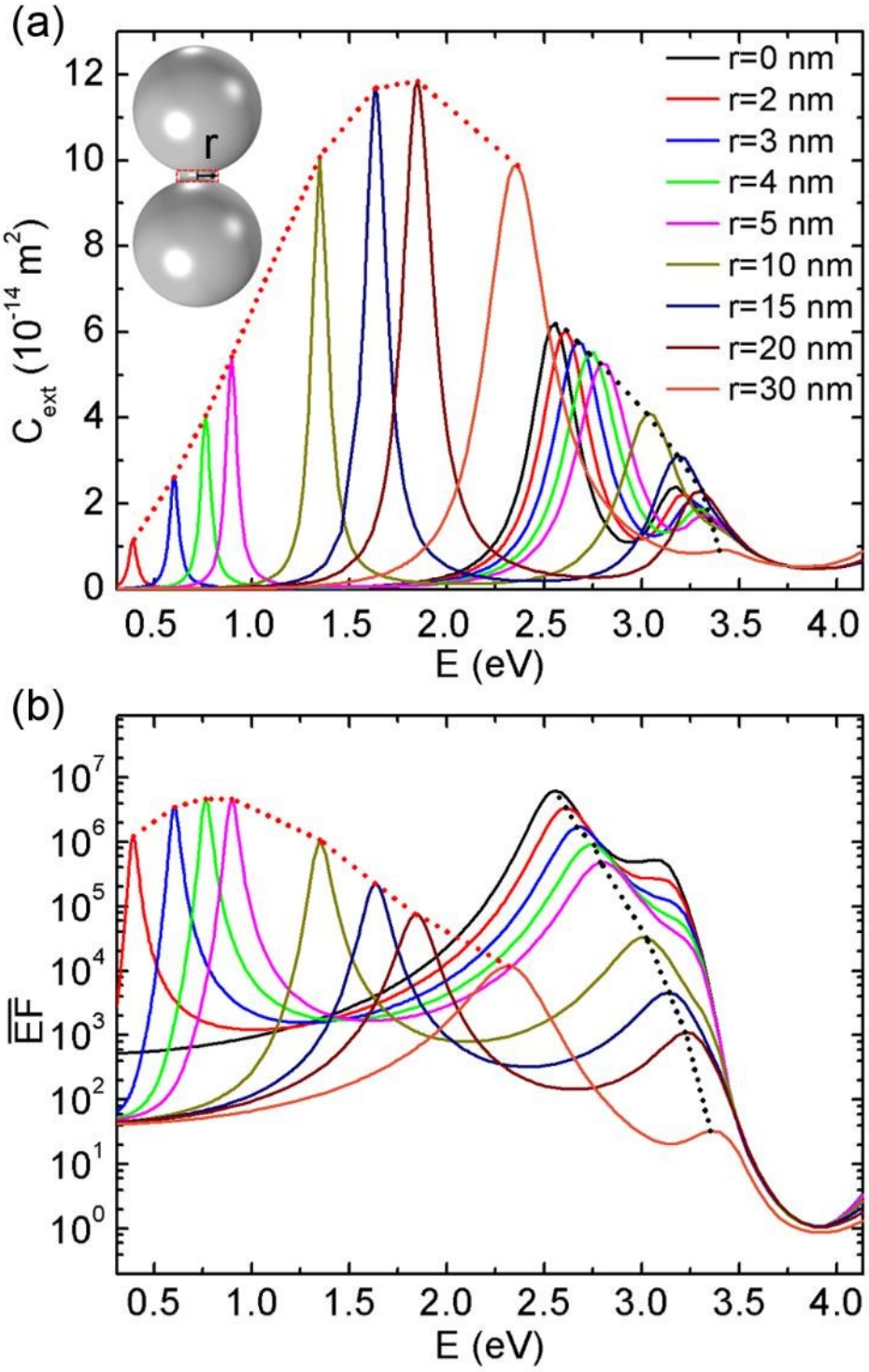

Fig. 1 Huang et al.

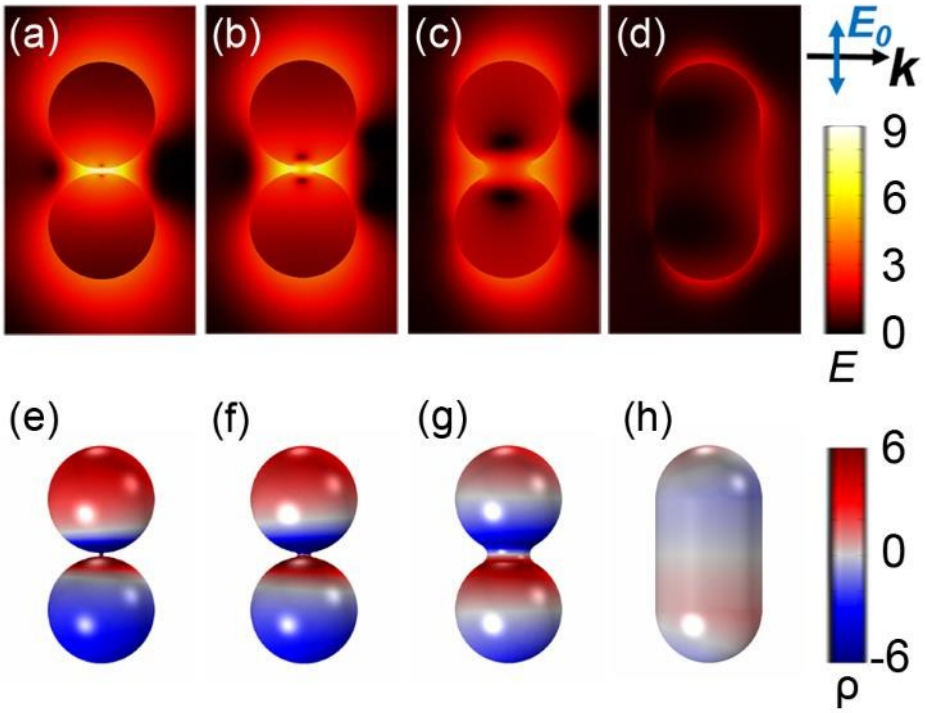

Fig. 2 Huang et al.

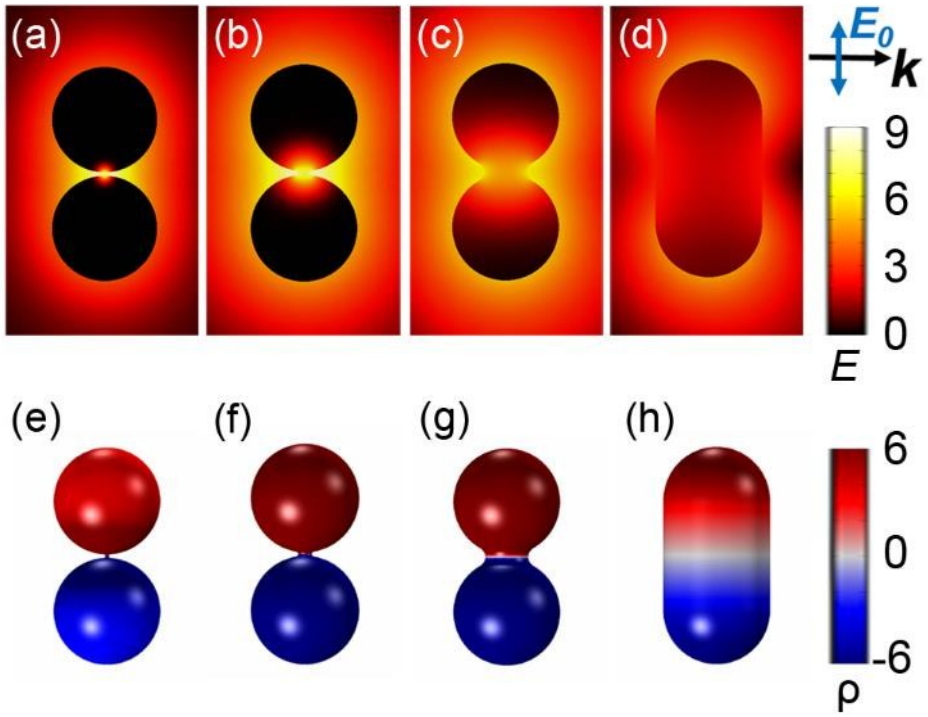

Fig. 3 Huang et al.

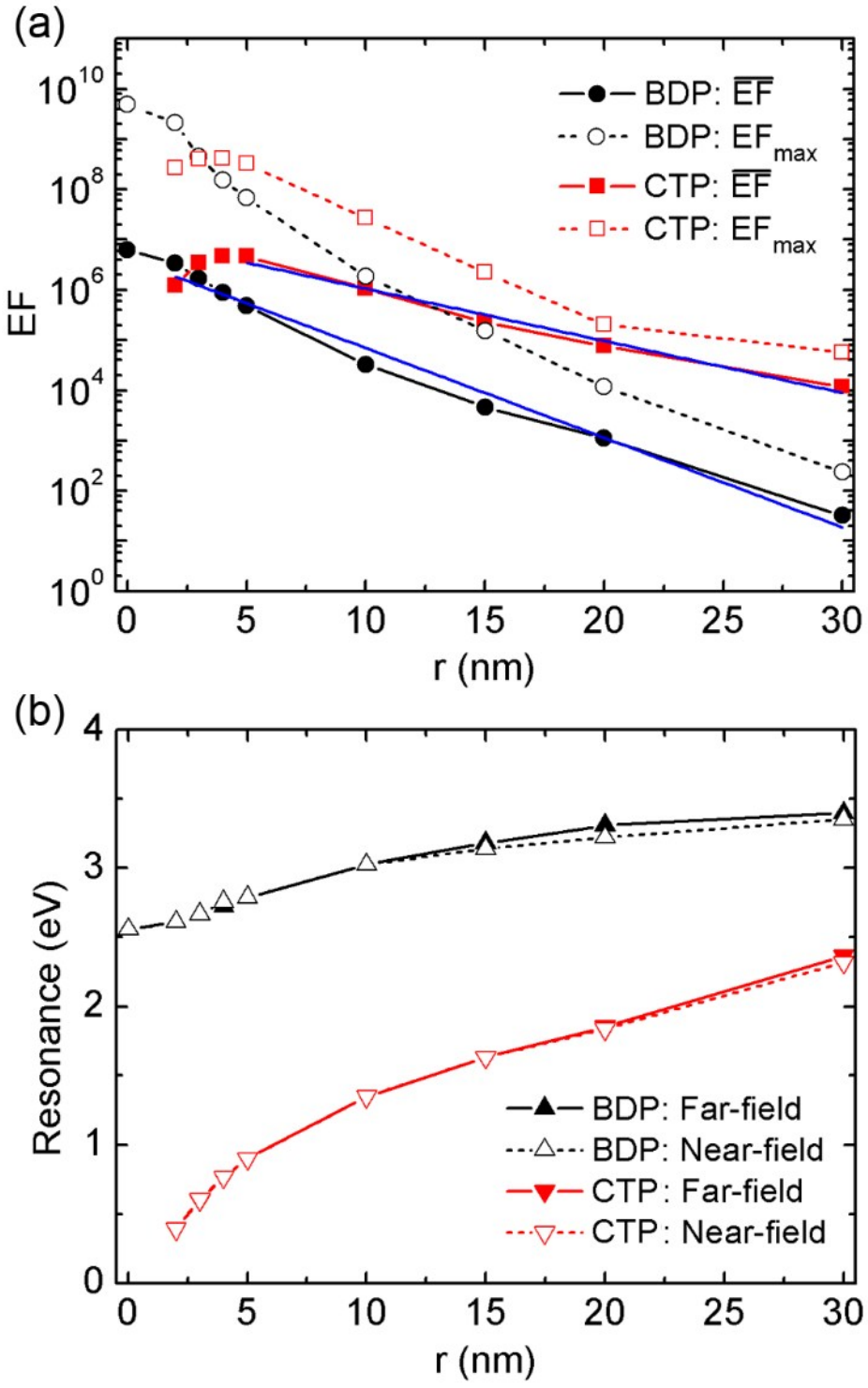

Fig. 4 Huang et al.